Published in final edited form as:
J Mol Cell Cardiol. 2013 April ; 57: 47–58. doi:10.1016/j.yjmcc.2012.11.013.

IN VIVO AND *IN VITRO* CARDIAC RESPONSES TO BETA-ADRENERGIC STIMULATION IN VOLUME-OVERLOAD HEART FAILURE

Anuradha Guggilam[1,2], **Kirk R Hutchinson**[1,3], **A Thomas West**[1], **Amy P Kelly**[1], **Maarten L Galantowicz**[1], **Amy J Davidoff**[4], **Sakthivel Sadayappan**[5], and **Pamela A Lucchesi**[1,2]

[1]Center for Cardiovascular and Pulmonary Research, The Research Institute at Nationwide Children's Hospital, Columbus, OH, USA

[2]Pediatrics, The Ohio state University, Columbus, OH, USA

[3]Department of Pharmacology, Louisiana State University Health Sciences Center, New Orleans, LA, USA

[4]Department of Biomedical Sciences, Division of Pharmacology, College of Osteopathic Medicine, University of New England, Biddeford, ME, USA

[5]Department of Cell and Molecular Physiology, Stritch School of Medicine, Loyola University Chicago, Maywood, IL, USA

1. Introduction

Volume overload (VO) results from increased preload on the heart, as occurs in regurgitant mitral and aortic valves, or ventricular septal defect. Left ventricular (LV) VO is characterized by eccentric hypertrophy with no change in wall thickness leading to an acute increase in wall stress. Eccentric hypertrophy during VO progression is associated with myocyte elongation via serial addition of sarcomeres and extracellular matrix degradation [1]. Several therapeutic agents, including ACE inhibitors [2], remain ineffective in treating VO induced heart failure (HF) owing to its distinct cardiac remodeling mechanisms. The cellular mechanisms that lead to myocyte failure have been extensively studied in human and animal models of pressure overload and myocardial infarction. Much less is known about the molecular and cellular mechanisms that underlie VO-induced HF. Our lab and others, using the aorto-caval fistula (ACF) rat model, have reported progressive LV pump failure associated with decreased myocyte contractility [3, 4].

Alterations in Ca^{2+} homeostasis contribute to the contractile dysfunction in various HF models. Changes in the expression and phosphorylation of a number of proteins involved in excitation-contraction (EC) coupling have been observed, including the sarcoplasmic reticulum (SR) ryanodine receptors (RyR), which are responsible for Ca^{2+}-induced Ca^{2+}

Corresponding author: Pamela A Lucchesi, PhD, 700 Children's drive, Center for Cardiovascular and Pulmonary Research, Nationwide Children's Hospital, Columbus, OH 43205, pamela.lucchesi@nationwidechildrens.org, Phone: 614-722-4969, Fax: 614-722-4881.

Disclosures: The authors declare no conflict of interest.

release, the phospholamban/SR Ca^{2+}-ATPase (SERCA2a) Ca^{2+} reuptake complex, the plasmalemmal Na^{+}/Ca^{2+} exchanger (NCX), myofilament proteins, as well as changes in β-adrenergic receptor density and signaling. However, the cellular mechanisms responsible for these changes in Ca^{2+} homeostasis are multifactorial. While some studies in human HF suggested that myocardial dysfunction was associated with reduced expression of L-type Ca^{2+} channels [5], others found a reduction in SERCA with an increase in NCX [6]. Previous studies in ACF-induced HF demonstrated decreased SERCA2a and RyR expression associated with reduced myocyte contractility [3].

Desensitization of the β_1-adrenergic receptor (β_1-AR) pathway is a hallmark of chronic HF [7] and leads to reduced intracellular calcium $[Ca^{2+}]_i$ cycling, contractility and myocardial energetics. The response of volume overloaded and failing myocytes to β_1-AR agonists under *in vivo* and *in vitro* conditions remains controversial. Dhalla's group [8] reported increased β_1-AR density in ACF hearts during the decompensated phase of HF, while Ding *et al* showed abrogated sarcomere shortening response to β-AR agonist at this stage [3]. However, neither study compared these results with measurements of *in vivo* LV functional responses to dobutamine and provided a limited assessment of sarcomeric and Ca^{2+}-binding proteins. In this study, we examined the effects of chronic end-stage VO and β-AR stimulation on LV structure and function as well as on isolated rat LV myocyte cellular and functional responses.

2. Methods

2.1. Animals

Male Sprague-Dawley rats (Harlan) weighing 250–300g were housed in a temperature and humidity controlled room using a 12h light/dark cycle and standard rat chow and water *ad libitum*. All studies conformed to the principles of the National Institutes of Health "Guide for the Care and Use of Laboratory Animals," (NIH publication No. 85-12, revised 1996). The protocol was approved by the Institutional Animal Care and Use Committee of The Research Institute at Nationwide Children's Hospital.

2.2. ACF surgery protocol

Cardiac volume overload was induced in rats under isoflurane anesthesia (2%) as described previously. Briefly, a midline abdominal incision was made and the abdominal aorta and inferior vena cava were exposed. An 18-g needle was inserted into the abdominal aorta and advanced into the inferior vena cava through the common midwall, creating an ACF. The needle was removed, and cyanoacrylate glue (Vetbond) was used to seal the aortic puncture. Shunt patency was confirmed by visualization of mixture of bright red arterial blood in the vena cava. The abdominal muscle and skin were closed using 5-0 chromic gut suture and 4-0 vicryl, respectively. Sham animals underwent similar procedure except no aortic puncture was made.

2.3. Echocardiography

Transthoracic echocardiograms (n=10 per group) were performed using a Toshiba Xario with a 12.5 mHz transducer under 1.5% isoflurane anesthesia, as described previously [9]. In brief, isovolumetric relaxation and contraction times (IVRT and IVCT, respectively) and aortic ejection time (ET) were obtained by pulsed wave Doppler at the mitral valve level. M-mode images were obtained at the level of the papillary muscles to assess chamber diameters in systole and diastole (LVDs and LVDd) and LV posterior wall thickness in systole and diastole (PWTs and PWTd, respectively). The following indices were calculated:

$$\%\ \text{fractional shortening (\%FS)} = (\text{LVDd-LVDs})/\text{LVDd} \times 100$$

Eccentric dilation index = (2xPWTd)/LVDd

Tei index = (IVRT+IVCT)/ET

2.4. Surface ECG Measurement

Rats were anesthetized with 2% via nosecone and body temperature was maintained at 37°C using a heat lamp. Lead II ECGs were recorded for 5 minutes with subcutaneous needle electrodes and an Iworx data acquisition system sampling at 1 kHz. Labscribe software (Iworx) was used for analysis of heart rate (HR), PR interval, QRS duration, QT interval, and QTc (corrected for heart rate).

2.5. Measurement of LV hemodynamics

LV hemodynamics were assessed *in vivo* using pressure-volume (PV) analysis [9]. Briefly, the rats were sedated with 3% isoflurane, intubated and were maintained under 2% isoflurane anesthesia throughout the procedure. PV catheter was introduced in to the LV via the right carotid artery. Following equilibration, baseline LV hemodynamic parameters were acquired using 8–10 consecutive PV loops. An inferior vena caval occlusion was used to measure changes in load-independent parameters, such as preload-recruitable stroke work (PRSW) and end-systolic pressure volume relationships (ESPVR). iWorx Labscribe 2 acquisition and analysis software was used to analyze the data.

The following parameters were used to measure LV systolic and diastolic function: stroke volume (SV), heart rate (HR), cardiac output (CO), percent ejection fraction (%EF), maximum and minimum dp/dt, LV end-systolic and end-diastolic volume (ESV and EDV), LV end-systolic and end-diastolic pressure (ESP and EDP), slope of the ESPVR, PRSW and relaxation constant (Tau Weiss).

2.6. LV myocyte isolation

Following 21-weeks of ACF surgery, viable LV myocytes were isolated as previously described [10]. Briefly, the heart was mounted on a Langendorff apparatus followed by retrograde perfusion through the aorta with perfusion buffer for 4 min, and a subsequent perfusion with buffer containing 12.5 μM $CaCl_2$0.14 mg/mL trypsin and 12 Wünsch units of Liberase TH (Roche) for 10–12 min. The LV was separated from the digested heart and myocytes were mechanically dispersed in perfusion buffer (containing 12.5 μM $CaCl_2$ and 10% calf serum) and filtered. The isolated myocytes were then resuspended in increasing concentrations of $CaCl_2$ over 16 min to achieve a final concentration of 1 mM. Isolated myocytes were plated on laminin coated cell-perfusion chambers in Minimal Essential Medium (MEM) with Hanks' salts and 2 mM L-glutamine (MEM), supplemented with 5% calf serum, 2,3-butanedione monoxime and 100 U/mL penicillin-streptomycin. After 1-hour incubation, plated myocytes were placed in culture medium (serum-free MEM with 0.1% BSA and 100 U/mL Pencillin-streptomycin).

2.7. Measurement of contractility and Ca^{2+}-transients in isolated LV myocytes

Contractility of the isolated LV myocytes was measured in myocytes within 2–3 hours of initial plating by mounting cell-perfusion chambers on an inverted Olympus IX-71 microscope and perfusing at 37°C with Tyrode's buffer. Isotonic sarcomere shortening was measured using an IonOptix Myocam camera (IonOptix Corporation, Milton, MA). Myocytes were perfused with Tyrode's solution ± 100 nM isoproterenol (Iso) to study β-adrenergic responsiveness. The following parameters were recorded: sarcomere peak shortening normalized to resting sarcomere length (%PS,), maximal velocity of cell shortening (+dL/dt) and maximal velocity of cell relengthening (−dL/dt,). Twitch duration

was measured from the beginning of myocyte contraction to 90% of peak amplitude ($TP_{90\%}$) and from peak amplitude to 90% relaxation ($TR_{90\%}$).

Ca^{2+} transients were measured by loading myocytes at room temperature with 0.5 μM Fura-2A (Molecular Probes, Eugene, OR) for 20 min. Excess dye was washed with serum-free MEM. After 20 mins, cells in MEM were washed with Tyrode's buffer and myocytes were field stimulated at 1 Hz. Fura-2A loaded cells were excited with 380±20 nm light during field stimulation and single cell fluorescent emission was collected at 510±20 nm. Immediately before and after field stimulation, myocytes were excited with 360±20 nm and 510 nm emissions were collected for ratiometric determinations.

Data were expressed as peak Ca^{2+} amplitude normalized to resting diastolic Ca^{2+} (bl% peak h), area under systolic Ca^{2+} signal normalized to peak height, (A_S/PK; representing Ca^{2+} available for contraction phase) and area under Ca^{2+} decay signal normalized to peak height, (A_D/PK; Ca^{2+} decay leading to relaxation). Maximum rates in rise of systolic Ca^{2+} and Ca^{2+} decay were derived from the Ca^{2+} recordings (±dV/dt). All measurements were analyzed using Ionwizard data acquisition system (IonOptix).

2.8. Immunoblot analysis

LV mid-wall tissue lysates were prepared, as described [2]. Proteins (15 μg) were separated by SDS-PAGE and transferred to PVDF membranes. Immunoblotting was performed with antibodies against ryanodine receptor (RyR, 1:1,000, generous gift from Dr. Andrew Marks), phospho-RyR Ser2808 (pRyR2808, 1:2,000, Abcam), phospholamban (PLB, 1:2,000, Millipore), phospho-PLB Ser16 (p-PLB, 1:2,000, Millipore), SERCA-2a (1:2,000, Thermo), β-MHC, cardiac troponin I (cTnI, 1:2,000, Sigma), phospho-TnI Ser23/24 (p-cTnI, 1:2,000, Cell Signaling), cardiac myosin binding protein-C (cMyBP-C) and phosphor-specific cMyBP-C Ser273, Ser-282 and Ser-302 (1:2,000, [11]), connexin-43 (Cx-43), phospho-Cx-43 Ser368 (pCx-43), N-cadherin (N-cad), Src, Zo-1 or ERK1/2 (1:5,000, Santa Cruz). Relative band densities were analyzed using GelEval (v1.22 Frog Dance Software) and were normalized to ERK1/2 loading controls.

2.9. Immunofluorescence microscopy

Immunofluorescence was performed as described [9]. Following antigen retrieval and blocking with 10% goat serum, slides were incubated overnight at 4°C with a rabbit polyclonal anti-Cx-43 (1:250, SantaCruz). For secondary labeling goat anti-rabbit Alexa-Fluor 488 (1:500, Invitrogen, Carlsbad, CA) conjugated IgG was used and sections were mounted and counter stained using Vectashield with DAPI (Vector Laboratories, Burlingame, CA).

2.9. Statistical Analysis

Data are expressed as mean±SEM. Statistical analyses were performed using GraphPad Prism V5.0 (GraphPad Software). Unpaired Student's t-tests or one-way ANOVA, followed by Bonferroni's post-hoc test, were used to measure differences between groups. $p<0.05$ was considered statistically significant.

3. Results

3.1. Chronic ACF-induced eccentric dilatation and LV remodeling

M-mode echocardiography demonstrated an increase in LV diameter while LV posterior wall thickness (LVPWT) remained unchanged at 21wks following ACF (Figure 1). Figure 1A shows a representative M-mode view of the LV in sham and ACF at 21-weeks post-surgery. ACF at 21 weeks was associated with an increase in LV diameter at systole and

diastole (LVEDd and LVEDs, respectively). The ratio of (2xPWTd)/LVDD, an index of eccentric dilatation, was significantly lower in ACF rats compared to sham rats (Figure 1C), indicating eccentric hypertrophy (Table 1). In addition, increased HW/BW and LW/BW ratios in the ACF rats (Table 2) suggested pathologic LV hypertrophy and pulmonary congestion. Baseline echocardiography at the beginning of the study depicted no changes in LV dimensions between sham and ACF groups (data not shown).

3.2. Chronic ACF modulated LV contractile function

Systolic function, assessed by echocardiography, showed a significant decline in %FS (29%) in ACF rats (Figure 2A), indicating contractile dysfunction. ACF also induced abnormal increases in the Doppler time intervals, IVCT and IVRT, with abbreviated ET resulting in an elevated Tei index, an indicator of global LV dysfunction (Figure 2B). In order to better understand the LV hemodynamics in VO-induced HF, we performed PV loop analysis. LV hemodynamic parameters are presented in Table 2. As expected, ACF increased LV EDV and ESV. Mean heart rate (HR) and mean arterial pressure (MAP) remained unchanged compared to sham. LV EF reflected a marked, 27% decrease in ACF vs. sham. Despite a significant ESV increase in ACF, ESP and dP/dt_{max} remained unchanged. SV was significantly increased in ACF, confirming that ACF induced a high output HF (Table 2). ESPVR was significantly decreased in ACF demonstrating marked systolic dysfunction (Figure 2B). EDV was almost doubled at 21-wks post ACF (99% increase) relative to sham. However, EDP and other diastolic relaxation parameters, Tau and dP/dt_{min}, did not differ from sham levels (Table 2).

3.3. Effect of VO on cardiomyocyte function and Ca^{2+} transients

Representative sarcomere contractility recordings are shown in Figure 3A. Compared to those of sham, a ~30% decrease in unloaded sarcomere peak shortening (%PS) was observed in freshly isolated ACF myocytes that were field stimulated at 1 Hz. Compared to sham, sarcomere shortening velocity (−dL/dt) and relaxation velocity (+dL/dt) were also reduced in ACF myocytes by ~40% and ~20%, respectively (Figure 3A).

To gain further insight into changes in excitation-contraction coupling, we next compared the amplitude and kinetics of the Ca^{2+} transient. Representative Ca^{2+} transients are shown in Figure 3B. The mean peak amplitude of Ca^{2+} fluorescence was higher in ACF myocytes compared to that of sham. This increase in Ca^{2+} peak amplitude in ACF was associated with significantly increased rates of rise and decay. No changes in time to peak 90% (TP 90%) and time to relaxation (TR 90%) were observed between sham and ACF myocytes (Table 3). We also integrated the Ca^{2+} signals during systole and leading to diastole, each normalized to peak amplitude (A_S/PK and A_D/PK, respectively, which account for the time course as well as the shape of the signal. These indices give a more appropriate estimate of Ca^{2+} available to support contraction and relaxation [12]. These indices were not different between sham and ACF suggesting that changes in peak amplitude were offset by increased Ca^{2+} kinetics.

We next examined alterations in the expression of SR Ca^{2+} regulatory proteins (Figure 4A). Western blot analysis indicated that the SR Ca^{2+} release channel RyR was down-regulated ~40%. However, RyR Ser-2808 phosphorylation was not different between groups, resulting in net RyR hyper-phosphorylation (i.e pRyR/RyR) in ACF. We were unable to detect RyR Ser-2815 phosphorylation in either sham or ACF at this time point. SERCA-2a, the SR protein responsible for re-uptake of $[Ca^{2+}]_i$ into the SR, was decreased by ~20% in ACF compared to sham LV. Total PLB was decreased in ACF, but PLB Ser-16 phosphorylation was slightly, but significantly increased in ACF, indicating a decreased inhibitory function towards SERCA-2a. Collectively, these results suggest that ACF myocytes exhibit

decreased contractility even though the mechanisms which regulate cytosolic Ca^{2+} during the contractile phase would, on balance, suggest that Ca^{2+} availability is not compromised.

We next RT-PCR and/or western blot analysis to assess the expression of myofilament proteins that regulate shortening kinetics or myofilament Ca^{2+} sensitivity, using (Figure 4B). The ratio of β-MHC to α-MHC mRNA was significantly increased in ACF compared to sham; this increase in the neonatal β-MHC isoform was confirmed at the protein level by western blotting. This neonatal form of MHC is an energy conserving slow-twitch isoform that has been shown to be overexpressed in several forms of HF in both humans and animals [13, 14]. Titin isoform expression, as well as desmin, and α/β-crystallin were unaltered by VO (data not shown). Cardiac TnI, a component of thin filament regulatory troponin complex to which $[Ca^{2+}]_i$ binds to initiate contraction, was decreased in ACF, while its phosphorylation at Ser-23/24 was unchanged. No changes in TnT were detected between sham and ACF (data not shown). Total MyBP-C protein levels were significantly downregulated in ACF compared to Sham. We also observed decreased phosphorylation of cMyBP-C at sites Ser-273, Ser-282 and Ser-302; however, when normalized to total cMyBP-C there were no differences in the ratio of phosphorylated to total cMyBP-C between sham and ACF.

3.4. *In vivo* and *in vitro* β-adrenergic responsiveness in VO

To further understand the mechanisms that underlie LV contractile dysfunction induced by ACF, we measured *in vivo* and *in vitro* responses to β-adrenergic stimulation. Dobutamine is commonly used clinically and experimentally to assess myocardial β-adrenergic responsiveness, while isoproterenol when administered *in vivo* can cause arrythmogenic and vascular side effects [15]. Therefore, in this study we followed the traditional dobutamine stress echo protocol. Figure 5A shows *in vivo* LV functional responses to dobutamine challenge as assessed by echocardiography. The positive chronotropic (increased HR) and inotropic effects (increased %FS) to dobutamine observed in sham were significantly attenuated in ACF. A similar response was observed in the LV hemodynamic measures, %EF and dP/dt_{max}, with a low dose infusion of dobutamine (data not shown).

Since the *in vivo* cardiac performance is influenced by persistent increases in circulating catecholamines in HF animals, we next challenged the isolated myocytes from these rats with Iso, a non-specific β-adrenergic agonist. Interestingly, ACF myocytes showed *preserved* responsiveness to Iso, as indicated by an 89% increase in %PS over baseline compared to a 53% increase in sham myocytes (Figure 5B). To rule out possible differences between effects of dobutamine use *in vivo* and Iso use *in vitro*, we performed a pilot study using Iso infusion *in vivo* and found similar results compared to dobutamine infusion (data not shown).

Iso caused an increase in $[Ca^{2+}]_i$ amplitude in sham but the response was absent in ACF myocytes. A_S/PK was not different between sham and ACF in response to Iso (data not shown). However, Ca^{2+} transient decay was faster after ISO as expected (i.e., smaller A_D/PK), and the response was similar in sham and ACF groups. Taken together, these results suggest that the changes in in pRyR and pPLB levels in ACF LV resulted in a maximal myocyte Ca^{2+} peak transient amplitude that could not be further augmented by Iso.

3.5. VO induced decreases in myocardial Cx-43 levels

We next compared β-adrenergic receptor (β-AR) expression and the organization and composition of gap junctions between sham and ACF. There was a significant decrease in β_1-AR mRNA in ACF compared to sham tissue and no changes in β_2-AR (Figure 6A). The protein expression and localization of the gap junction protein Cx-43 and the intercalated

disk proteins N-cadherin (N-Cad) or zona occluden-1 (ZO-1) were detected by immunofluorescence and/or immunoblotting. Cx-43 expression was markedly diminished in ACF LV despite preserved N-cad levels (Figure 6B). Furthermore, Cx-43 expression in ACF LV lysates was decreased by ~55% compared to sham LV lysates. There was no difference in ser-368 phosphorylation of Cx-43 between groups, resulting in increased levels of pCx-43/total Cx-43. These changes in Cx-43 were associated with an increase in QT interval (data not shown) and QTc as assessed by EKG (Figure 6B). No other significant differences in QRS or PR interval were detected (data not shown).

We also measured the expression of proteins that modulate Cx-43 expression at the gap junction (i.e., c-Src and ZO-1). c-Src is a tyrosine kinase involved in tyrosine phosphorylation of Cx-43 in myocytes inducing pore closure and channel degradation, while ZO-1 stabilizes Cx-43 in the gap junction. c-Src expression was increased, while ZO-1 levels were decreased in the LV of ACF rats (Figure 6C).

4. Discussion

In the present study we characterized LV structure and function, as well as isolated myocyte excitation-contraction coupling, at end-stage VO HF. We show for the first time that isolated cardiomyocytes in VO-induced HF remain responsive to β-adrenergic agonists, while the LV myocardium displayed expected decreases in β-adrenergic responsiveness *in vivo*. The key findings of this study are that end-stage VO results in: 1) a decline in LV systolic function that was coincident with changes in LV myocyte contractility, 2) altered E-C coupling dynamics with altered expression of $[Ca^{2+}]_i$ handling proteins and myofilaments, 3) a decline in *in vivo* β-adrenergic responsiveness that, interestingly, was preserved in isolated LV myocytes despite depressed basal cardiac myocyte contractility and 4) decreased levels of Cx-43.

We recently characterized the pathophysiological progression of HF caused by ACF induced VO [9]. Here, we show that end-stage VO-induced HF in this model was characterized by dilated hearts with eccentric hypertrophy and no changes in LVPWT. The dilatation of the LV correlated with eccentric myocyte hypertrophy (elongation of myocytes by addition of sarcomeres in series) and extracellular matrix degradation [1]. A similar pattern of dilated cardiomyopathy (DCM) is seen clinically in cases of anemia, mitral/aortic valve regurgitation or non-restricted ventricular septal defects [1]. These structural changes resulted in significantly elevated end-systolic and diastolic volumes leading to marked systolic dysfunction. Despite the substantial increase in LV volumes, end-systolic and diastolic filling pressures remained unchanged, likely due to the increased LV compliance. Signs of pulmonary edema and ascites observed at this stage likely result from excessive pre-load and signify HF symptoms and severe LV decompensation [16]. Reduced %FS (Figure 2A) and a decrease in the slope of ESPVR (Figure 2B) indicate marked systolic dysfunction. However, no evidence of diastolic dysfunction was observed.

In agreement with the *in vivo* data, isolated myocytes from ACF hearts exhibited reduced cell contractility along with depressed maximal velocities of shortening and relaxation. Based on various models of heart failure, these functional changes are likely, due to changes either in Ca^{2+} homeostasis, myofilament isoform expression or Ca^{2+} sensitivity. Contrary to what would be predicted by the mechanical data (whole hearts and isolated myocytes) Ca^{2+} transient in ACF myocytes, exhibited an increase in peak $[Ca^{2+}]_i$-amplitude with accelerated $[Ca^{2+}]_i$ kinetics. These changes in ACF myocytes were coincident with a ~20% decrease in SERCA-2a protein levels, and increased Ser-16 phosphorylation of PLB and Ser-2808 of the RyR, but no changes in NCX protein levels (data not shown). These phosphorylation domains are major regulatory sites for protein kinase A (PKA). The small but significant

reduction in SERCA-2a levels would be incongruent with accelerated decay of Ca^{2+} transients, however, increased in PLB phosphorylation observed may, in part, explain enhanced Ca^{2+} kinetics [17], and suggest a net compensation of SERCA-2a function. The fact that the myocyte pacing data at higher frequencies indicated no changes in Ca^{2+} relaxation kinetics (data not shown) further corroborates the compensated SERCA-2a function. This is further confirmed by no change in SERCA-2a/PLB ratio between sham and ACF. These findings are in contrary with those of Juric *et al.* 18] who found unaltered SERCA levels but reduced phosphorylation levels of PLB after 28 wks of ACF induction in rats. However, these discrepancies might be attributed to the difference in shunt size and therefore a dissimilar temporal progression of HF. Our lab, along with several others, observed an increased Ser-2808 phosphorylation of RyR relating to increased SR $[Ca^{2+}]_i$ leak in ACF myocytes [18–20]. Contrary to this, Juric et al observed an increase in the protein levels of FKBP 12.6 that is thought to stabilize RyR in its conformation. The mechanisms that underlie increased basal phosphorylation are unclear, but may reflect an increase in PKA activity [21, 22] and/or a decrease in protein phosphatase-1 (PP1) expression [17]. Recent evidence shows that Ser-2815 phosphorylation of RyR, a major regulatory site for CAMKII, is enhanced by excessive β-adrenergic stimulation resulting from chronic sympathoexcitation in chronic HF animals [23, 24]. However, we did not detect any levels of Ser-2815 phosphorylation of RyR at this stage in either normal or failing hearts. Taken together, the peak amplitude and kinetics of the Ca^{2+} transients appear to be dissociated from impaired mechanical function, however, these data suggest that the increased Ca^{2+} peak amplitude may be secondary to changes in phosphorylation-dependent Ca^{2+} leak from the RyR [25, 26].

Increased RyR phosphorylation and reduced SERCA-2a could contribute to the observed decreases in contractility rates (%PS, +dL/dt and −dL/dt) in ACF myocytes. To explore these links, we determined the time courses and amplitude of $[Ca^{2+}]_i$ transients during electrically-evoked contractions. We calculated areas under the curve for systolic Ca^{2+} (A_S/PK) and diastolic Ca^{2+} decay (A_D/PK) to provide an estimate of the total $[Ca^{2+}]_i$ available during the contraction and relaxation phases, respectively [12]. These calculations indicated that the amount of available $[Ca^{2+}]_i$ to the myofilaments during contraction or relaxation phases remained unchanged in ACF as compared to sham. Furthermore, no changes were noted in diastolic $[Ca^{2+}]_i$ between groups. Collectively, these results suggest that impaired $[Ca^{2+}]_i$ handling is not the predominate cause of the observed decrease in myocyte shortening in response to VO HF.

These results are distinct from those reported for other types of HF. For example, alterations in $[Ca^{2+}]_i$ cycling have been shown to underlie the contractile dysfunction in HF due to pressure overload or myocardial infarction. In human and various animal models of HF, diastolic calcium overload is a causative factor in the pathology of HF (7, 18). These diastolic $[Ca^{2+}]_i$ levels in HF typically arise from decreased removal of $[Ca^{2+}]_i$ due to depressed SERCA-2a activity, reduced expression/phosphorylation of PLB, and/or increased NCX levels [27, 28]. Enhanced SR leak via hyperphosphorylated RyRs also amplified the diastolic $[Ca^{2+}]_i$ levels [29]. These factors collectively slow the $[Ca^{2+}]_i$ clearing rate from the cytoplasm.

To further understand the mechanisms for decreased contractility, we compared the composition of myofilaments. Increased stretch (i.e. VO) initiates fetal re-programming of genes resulting in changes in the isoform of contractile proteins, which has been associated with decreased contractility in failing hearts [30]. The most characterized change is a shift in the myosin heavy chain isoform from the high ATPase α-MHC to the slower, but more energy efficient β-MHC isoform, which has been correlated with reduced contractility in patients with DCM [13]. A similar switch in MHC isoform is also found in cardiac

hypertrophy induced by myocardial infarction [31] and pressure overload [32, 33]. Increases in β-MHC result in slower cross-bridge cycling and decreased contractile kinetics. The decreased myocyte contractility and velocities of shortening and relaxation observed in ACF may be ascribed to the increased neonatal β-MHC form of myosin heavy chain expressed in the LV (Figure 7A).

Alterations in myofilament Ca^{2+} sensitivity also lead to contractile dysfunction. A number of processes that regulate Ca^{2+} binding to troponin C, and the resultant de-inhibition of actin and myosin interaction, alter myofilament Ca^{2+} sensitivity and force production. Under physiological conditions, myofilament Ca^{2+} sensitivity changes from beat to beat in response to ventricular filling causing changes in force production and accounts for the Frank-Starling mechanism. However, long lasting changes in Ca^{2+} sensitivity occur via a different mechanism involving PKA dependent phosphorylation of cTnI. Serine phosphorylation of cTnI at sites 23/24 decreases Ca^{2+} sensitivity thereby contributing to lusitropic response of β-adrenergic agonists [34, 35]. We observed a decrease in cTnI levels in ACF myocardium, however, no changes in phosphorylation levels of cTnI were observed. cMyBP-C, thick-filament accessory protein found in the A bands in myocardial sarcomeres and maintains sarcomere integrity and contraction during adrenergic stimulation [36]. Changes in cMyBP-C phosphorylation serve as a key coordinating point for sarcomere contraction by regulating cross-bridge formation. In particular hierarchal phosphorylation of Ser-282 by ribosomal S6 kinase, PKA or CaMKII is prerequisite for further phosphorylation at the Ser-273 and Ser-302 sites and is a key regulator of contractility and sarcomeric organization [37]. On the other hand, dephosphorylation of cMyBP-C, which accelerates its degradation, has been shown to be associated with the development of heart failure in animals and humans [38–40]. In the present study, we show for the first time that cMyBP-C protein levels were significantly decreased in volume overload induced heart failure in rats; although we also observed an apparent decrease in phosphorylation at the Ser-273, 282 and 302 sites, there were no differences in the ratio of phosphorylated to total cMyBP-C between Sham and ACF, suggesting that phosphorylation of cMyBP-C in ACF remained intact. Decreases in cMyBP-C expression are associated with LV contractile dysfunction and chamber dilation (Chen PP et al 2012), and cMyBP-C truncation mutations that cause decreased sarcomeric incorporation have been linked to human hypertrophic cardiomyopathy [41].

Collectively, the isolated myocyte data indicate a decreased contractility secondary to myofilament alterations despite compensated $[Ca^{2+}]_i$ homeostasis. The observed decrease in contractile reserve of the myocardium in response to challenge with the β-AR agonist, dobutamine, provides further evidence of LV contractile dysfunction in VO-induced HF. Surprisingly, both sham and ACF myocytes elicited a typical inotropic response to Iso as reflected by an increase in the amplitude and kinetics of cell shortening, despite reduced β_1-AR mRNA in ACF. Although we did not measure β-AR density at the protein level, Dhalla's group reported no changes in β_2-AR density and variable changes in β_1-AR, with a ~20% decrease at end-stage in this model [42, 43]. Given that Iso potentiated myocyte fractional shortening in both sham and ACF mycoytes, and pilot studies showed that Iso elicited the same increase in p-Ser23/24 cTnI (PKA phosphorylation site), the *in vivo* responses are not likely accounted for only by a change in β_1-AR protein. A similar conclusion was drawn a number of years ago by Communal et al [44]. It should also be recognized that isotonic contractions of cardiomyocytes do not always adequately reflect a working heart. For example, in our study, the inotropic (and lusitropic) effects of Iso were preserved in isolated myocytes but not *in vivo*.

On the contrary, Ding et al., showed that cardiomyocytes isolated from 10 week ACF rats still exhibited abrogated contractile response to Iso due to reduced Ca^{2+} stores and

decreased SERCA and RyR [3]. However, their study in non-failing hearts did not evaluate the phosphorylation levels of RyR and PLB. Our data show that differences in phosphorylated RyR receptor at baseline resulted in increased Ca^{2+} transient amplitude and kinetics were not further potentiated by Iso (Δ7% in ACF versus Δ55% in Sham, Table 3). Taken together these results suggest that increased basal phosphorylation of RyR offsets decreases in the basal expression of SERCA-2a and RyR, and PLB phosphorylation was sufficient to restore diastolic Ca^{2+} to basal levels and normalize the amount of Ca^{2+} available for subsequent contraction. However, in the face of β-AR stimulation, a different scenario emerges in which PKA cannot further increase RyR and PLB phosphorylation, but is able to increase contractility via phosphorylation of myofilament regulatory proteins. The finding that basal phosphorylation of cTnI was unchanged between sham and ACF lends support to this notion. Further studies are required to examine the balance between kinase and phosphatase signaling domains in this VO model of chronic HF.

To further explore the discrepancy between the *in vitro* and *in vivo* responses to β-AR stimulation in end-stage HF myocardium, we examined the expression of proteins involved in electromechanical transmission via cell-cell coupling. Cx-43, a major gap junction protein in the LV, was down-regulated in the ACF at the intercalated disc, while the tight junction protein, N-cadherin remained unchanged. There was no evidence of Cx-43 lateralization. Significant down-regulation and altered localization of Cx-43 from gap junction is observed in several HF models [45–47]. We also studied proteins that play a role in stabilization or degradation of Cx-43. ZO-1 is a membrane bound guanylate kinase that stabilizes Cx-43 at the gap junction plaque through cytoskeletal anchoring. Disruption of ZO-1 leads to altered stabilization of the gap junction plaque equilibrium between the two adjacent cells leading to plaque internalization [48]. Increased tyrosine phosphorylation by c-Src tyrosine kinase dissociates Cx-43/ZO-1 interaction, leading to inhibition of cell-cell communication in a model of cardiomyopathy [49]. Upregulation of c-Src by VO may be contributing to the observed loss of ZO-1 and subsequent loss of Cx-43 in the myocardium. These changes in reduced Cx-43 expression and phosphorylation were associated with increased QTc. Recent study shown the role of neuroglin-1β in restoring Cx-43 and reduction in QTc in a ACF induced VO [50]. These changes can also result in diminished propagation of Ca^{2+} waves [49] and may underlie reduced contractility and abrogated β-AR responsiveness seen in VO HF. In human HF, a negative correlation has been observed between QTc and systolic function of the heart [51]. Further studies are warranted to understand the role of connexins in altered Ca^{2+} wave propagation in cardiac dysfunction in volume overload heart failure.

The results from the present study suggest that despite the presence of intact, intrinsic myocyte contractile capacity, VO-induced HF results in reduced LV contractility due to alterations in myofilament Ca^{2+} sensitivity and reduced cell-cell communication resulting from altered protein turnover at the intercalated disc. Thus, these results suggest that therapeutic agents that increase Ca^{2+} sensitivity and Cx-43 expression at the intercalated disc may be possible targets for VO induced HF.

Acknowledgments

The study was supported by National Heart, Lung and Blood Institute 2R01HL056046 and 2R01HL63318 (PAL) and American Heart Association Postdoctoral Fellowship (AG), and funds provided by The Heart Center and Research Institute at Nationwide Children's Hospital.

REFERENCES

1. Carabello BA. Models of volume overload hypertrophy. J Card Fail. 1996; 2:55–64. [PubMed: 8798106]

2. Ryan TD, Rothstein EC, Aban I, Tallaj JA, Husain A, Lucchesi PA, et al. Left ventricular eccentric remodeling and matrix loss are mediated by bradykinin and precede cardiomyocyte elongation in rats with volume overload. J Am Coll Cardiol. 2007; 49:811–821. [PubMed: 17306712]

3. Ding YF, Brower GL, Zhong Q, Murray D, Holland M, Janicki JS, et al. Defective intracellular Ca2+ homeostasis contributes to myocyte dysfunction during ventricular remodelling induced by chronic volume overload in rats. Clin Exp Pharmacol Physiol. 2008; 35:827–835. [PubMed: 18346170]

4. Juric D, Yao X, Thandapilly S, Louis X, Cantor E, Chaze B, et al. Defects in ryanodine receptor function are associated with systolic dysfunction in rats subjected to volume overload. Exp Physiol. 2010; 95:869–879. [PubMed: 20472646]

5. Takahashi T, Allen PD, Lacro RV, Marks AR, Dennis AR, Schoen FJ, et al. Expression of dihydropyridine receptor (Ca2+ channel) and calsequestrin genes in the myocardium of patients with end-stage heart failure. J Clin Invest. 1992; 90:927–935. [PubMed: 1326001]

6. Hasenfuss G, Schillinger W, Lehnart SE, Preuss M, Pieske B, Maier LS, et al. Relationship between Na+-Ca2+-exchanger protein levels and diastolic function of failing human myocardium. Circulation. 1999; 99:641–648. [PubMed: 9950661]

7. Chidsey CA, Braunwald E, Morrow AG, Mason DT. Myocardial Norepinephrine Concentration in Man. Effects of Reserpine and of Congestive Heart Failure. N Engl J Med. 1963; 269:653–658. [PubMed: 14050968]

8. Wang X, Sentex E, Saini HK, Chapman D, Dhalla NS. Upregulation of beta-adrenergic receptors in heart failure due to volume overload. Am J Physiol Heart Circ Physiol. 2005; 289:H151–H159. [PubMed: 15734891]

9. Hutchinson KR, Guggilam A, Cismowski MJ, Galantowicz ML, West TA, Stewart JA Jr, et al. Temporal pattern of left ventricular structural and functional remodeling following reversal of volume overload heart failure. J Appl Physiol. 2011; 111:1778–1788. [PubMed: 21885799]

10. Shenouda SK, Lord KC, McIlwain E, Lucchesi PA, Varner KJ. Ecstasy produces left ventricular dysfunction and oxidative stress in rats. Cardiovasc Res. 2008; 79:662–670. [PubMed: 18495670]

11. Govindan S, McElligott A, Muthusamy S, Nair N, Barefield D, Martin JL, et al. Cardiac myosin binding protein-C is a potential diagnostic biomarker for myocardial infarction. J Mol Cell Cardiol. 2012; 52:154–164. [PubMed: 21971072]

12. Wold LE, Dutta K, Mason MM, Ren J, Cala SE, Schwanke ML, et al. Impaired SERCA function contributes to cardiomyocyte dysfunction in insulin resistant rats. J Mol Cell Cardiol. 2005; 39:297–307. [PubMed: 15878173]

13. Nakao K, Minobe W, Roden R, Bristow MR, Leinwand LA. Myosin heavy chain gene expression in human heart failure. J Clin Invest. 1997; 100:2362–2370. [PubMed: 9410916]

14. Miyata S, Minobe W, Bristow MR, Leinwand LA. Myosin heavy chain isoform expression in the failing and nonfailing human heart. Circ Res. 2000; 86:386–390. [PubMed: 10700442]

15. Tuttle RR, Mills J. Dobutamine: development of a new catecholamine to selectively increase cardiac contractility. Circ Res. 1975; 36:185–196. [PubMed: 234805]

16. Swynghedauw B, Baillard C. Biology of hypertensive cardiopathy. Curr Opin Cardiol. 2000; 15:247–253. [PubMed: 11139087]

17. Lompre AM, Hajjar RJ, Harding SE, Kranias EG, Lohse MJ, Marks AR. Ca2+ cycling and new therapeutic approaches for heart failure. Circulation. 2010; 121:822–830. [PubMed: 20124124]

18. Juric D, Yao X, Thandapilly S, Louis X, Cantor E, Chaze B, et al. Defects in ryanodine receptor function are associated with systolic dysfunction in rats subjected to volume overload. Experimental Physiology. 2010; 95:869–879. [PubMed: 20472646]

19. Hisamatsu Y, Ohkusa T, Kihara Y, Inoko M, Ueyama T, Yano M, et al. Early changes in the functions of cardiac sarcoplasmic reticulum in volume-overloaded cardiac hypertrophy in rats. J Mol Cell Cardiol. 1997; 29:1097–1109. [PubMed: 9160862]

20. Ding YF, Brower GL, Zhong Q, Murray D, Holland M, Janicki JS, et al. Defective intracellular Ca2+ homeostasis contributes to myocyte dysfunction during ventricular remodelling induced by chronic volume overload in rats. Clin Exp Pharmacol Physiol. 2008; 35:827–835. [PubMed: 18346170]

21. Oda T, Yano M, Yamamoto T, Tokuhisa T, Okuda S, Doi M, et al. Defective regulation of interdomain interactions within the ryanodine receptor plays a key role in the pathogenesis of heart failure. Circulation. 2005; 111:3400–3410. [PubMed: 15967847]
22. Wehrens XH, Lehnart SE, Reiken S, Vest JA, Wronska A, Marks AR. Ryanodine receptor/calcium release channel PKA phosphorylation: a critical mediator of heart failure progression. Proc Natl Acad Sci U S A. 2006; 103:511–518. [PubMed: 16407108]
23. Wang W, Zhu W, Wang S, Yang D, Crow MT, Xiao RP, et al. Sustained beta1-adrenergic stimulation modulates cardiac contractility by Ca2+/calmodulin kinase signaling pathway. Circ Res. 2004; 95:798–806. [PubMed: 15375008]
24. Ai X, Curran JW, Shannon TR, Bers DM, Pogwizd SM. Ca2+/calmodulin-dependent protein kinase modulates cardiac ryanodine receptor phosphorylation and sarcoplasmic reticulum Ca2+ leak in heart failure. Circ Res. 2005; 97:1314–1322. [PubMed: 16269653]
25. Marx SO, Reiken S, Hisamatsu Y, Jayaraman T, Burkhoff D, Rosemblit N, et al. PKA phosphorylation dissociates FKBP12.6 from the calcium release channel (ryanodine receptor): defective regulation in failing hearts. Cell. 2000; 101:365–376. [PubMed: 10830164]
26. Bers DM, Eisner DA, Valdivia HH. Sarcoplasmic reticulum Ca2+ and heart failure: roles of diastolic leak and Ca2+ transport. Circ Res. 2003; 93:487–490. [PubMed: 14500331]
27. Pogwizd SM, Qi M, Yuan W, Samarel AM, Bers DM. Upregulation of Na+/Ca2+ Exchanger Expression and Function in an Arrhythmogenic Rabbit Model of Heart Failure. Circulation Research. 1999; 85:1009–1019. [PubMed: 10571531]
28. O'Rourke B, Kass DA, Tomaselli GF, Kääb S, Tunin R, Marbán E. Mechanisms of Altered Excitation-Contraction Coupling in Canine Tachycardia-Induced Heart Failure, I : Experimental Studies. Circulation Research. 1999; 84:562–570. [PubMed: 10082478]
29. Jiang MT, Lokuta AJ, Farrell EF, Wolff MR, Haworth RA, Valdivia HH. Abnormal Ca2+ Release, but Normal Ryanodine Receptors, in Canine and Human Heart Failure. Circulation Research. 2002; 91:1015–1022. [PubMed: 12456487]
30. Stelzer JE, Brickson SL, Locher MR, Moss RL. Role of myosin heavy chain composition in the stretch activation response of rat myocardium. J Physiol. 2007; 579:161–173. [PubMed: 17138609]
31. Hart DL, Heidkamp MC, Iyengar R, Vijayan K, Szotek EL, Barakat JA, et al. CRNK gene transfer improves function and reverses the myosin heavy chain isoenzyme switch during postmyocardial infarction left ventricular remodeling. J Mol Cell Cardiol. 2008; 45:93–105. [PubMed: 18495152]
32. Li XM, Ma YT, Yang YN, Liu F, Chen BD, Han W, et al. Downregulation of survival signalling pathways and increased apoptosis in the transition of pressure overload-induced cardiac hypertrophy to heart failure. Clin Exp Pharmacol Physiol. 2009; 36:1054–1061. [PubMed: 19566828]
33. James J, Hor K, Moga MA, Martin LA, Robbins J. Effects of myosin heavy chain manipulation in experimental heart failure. J Mol Cell Cardiol. 2010; 48:999–1006. [PubMed: 19854200]
34. Zhang R, Zhao J, Mandveno A, Potter JD. Cardiac troponin I phosphorylation increases the rate of cardiac muscle relaxation. Circ Res. 1995; 76:1028–1035. [PubMed: 7758157]
35. Li L, Desantiago J, Chu G, Kranias EG, Bers DM. Phosphorylation of phospholamban and troponin I in beta-adrenergic-induced acceleration of cardiac relaxation. Am J Physiol Heart Circ Physiol. 2000; 278:H769–H779. [PubMed: 10710345]
36. McClellan G, Kulikovskaya I, Winegrad S. Changes in cardiac contractility related to calcium-mediated changes in phosphorylation of myosin-binding protein C. Biophys J. 2001; 81:1083–1092. [PubMed: 11463649]
37. Sadayappan S, Gulick J, Osinska H, Barefield D, Cuello F, Avkiran M, et al. A critical function for Ser-282 in cardiac Myosin binding protein-C phosphorylation and cardiac function. Circ Res. 2011; 109:141–150. [PubMed: 21597010]
38. Yuan C, Guo Y, Ravi R, Przyklenk K, Shilkofski N, Diez R, et al. Myosin binding protein C is differentially phosphorylated upon myocardial stunning in canine and rat hearts-- evidence for novel phosphorylation sites. Proteomics. 2006; 6:4176–4186. [PubMed: 16791825]

39. Sadayappan S, Gulick J, Osinska H, Martin LA, Hahn HS, Dorn GW 2nd, et al. Cardiac myosin-binding protein-C phosphorylation and cardiac function. Circ Res. 2005; 97:1156–1163. [PubMed: 16224063]
40. van Dijk SJ, Dooijes D, dos Remedios C, Michels M, Lamers JM, Winegrad S, et al. Cardiac myosin-binding protein C mutations and hypertrophic cardiomyopathy: haploinsufficiency, deranged phosphorylation, and cardiomyocyte dysfunction. Circulation. 2009; 119:1473–1483. [PubMed: 19273718]
41. Marston S, Copeland O, Jacques A, Livesey K, Tsang V, McKenna WJ, et al. Evidence from human myectomy samples that MYBPC3 mutations cause hypertrophic cardiomyopathy through haploinsufficiency. Circ Res. 2009; 105:219–222. [PubMed: 19574547]
42. Wang X, Sentex E, Saini HK, Chapman D, Dhalla NS. Upregulation of beta-adrenergic receptors in heart failure due to volume overload. Am J Physiol Heart Circ Physiol. 2005; 289:H151–H159. [PubMed: 15734891]
43. Sethi R, Saini HK, Guo X, Wang X, Elimban V, Dhalla NS. Dependence of changes in beta-adrenoceptor signal transduction on type and stage of cardiac hypertrophy. J Appl Physiol. 2007; 102:978–984. [PubMed: 17122376]
44. Communal C, Ribuot C, Durand A, Demenge P. Myocardial beta-adrenergic reactivity in volume overload-induced cardiac hypertrophy in the rat. Fundam Clin Pharmacol. 1998; 12:411–419. [PubMed: 9711463]
45. Teunissen BE, Jongsma HJ, Bierhuizen MF. Regulation of myocardial connexins during hypertrophic remodelling. Eur Heart J. 2004; 25:1979–1989. [PubMed: 15541833]
46. Fernandez-Cobo M, Gingalewski C, Drujan D, De Maio A. Downregulation of connexin 43 gene expression in rat heart during inflammation. The role of tumour necrosis factor. Cytokine. 1999; 11:216–224. [PubMed: 10209069]
47. Emdad L, Uzzaman M, Takagishi Y, Honjo H, Uchida T, Severs NJ, et al. Gap junction remodeling in hypertrophied left ventricles of aortic-banded rats: prevention by angiotensin II type 1 receptor blockade. J Mol Cell Cardiol. 2001; 33:219–231. [PubMed: 11162128]
48. Gilleron J, Carette D, Fiorini C, Benkdane M, Segretain D, Pointis G. Connexin 43 gap junction plaque endocytosis implies molecular remodelling of ZO-1 and c-Src partners. Commun Integr Biol. 2009; 2:104–106. [PubMed: 19704902]
49. Toyofuku T, Yabuki M, Otsu K, Kuzuya T, Tada M, Hori M. Functional role of c-Src in gap junctions of the cardiomyopathic heart. Circ Res. 1999; 85:672–681. [PubMed: 10521240]
50. Wang XH, Zhuo XZ, Ni YJ, Gong M, Wang TZ, Lu Q, et al. Improvement of cardiac function and reversal of gap junction remodeling by Neuregulin-1beta in volume-overloaded rats with heart failure. J Geriatr Cardiol. 2012; 9:172–179. [PubMed: 22916065]
51. Davey P. QT interval lengthening in cardiac disease relates more to left ventricular systolic dysfunction than to autonomic function. Eur J Heart Fail. 2000; 2:265–271. [PubMed: 10938487]

Research highlights

- A decline in LV contractility in VO HF is coincident with that of LV myocytes
- $[Ca^{2+}]_i$ levels were offset by EC coupling proteins with no net effect on function
- Changes in myofilament proteins contribute to reduced contractility in HF
- β-AR responsiveness was Decreased *in vivo* HF but preserved in isolated myocytes
- Reduced connexin-43 contributes to altered basal and β-AR responsiveness in VO HF

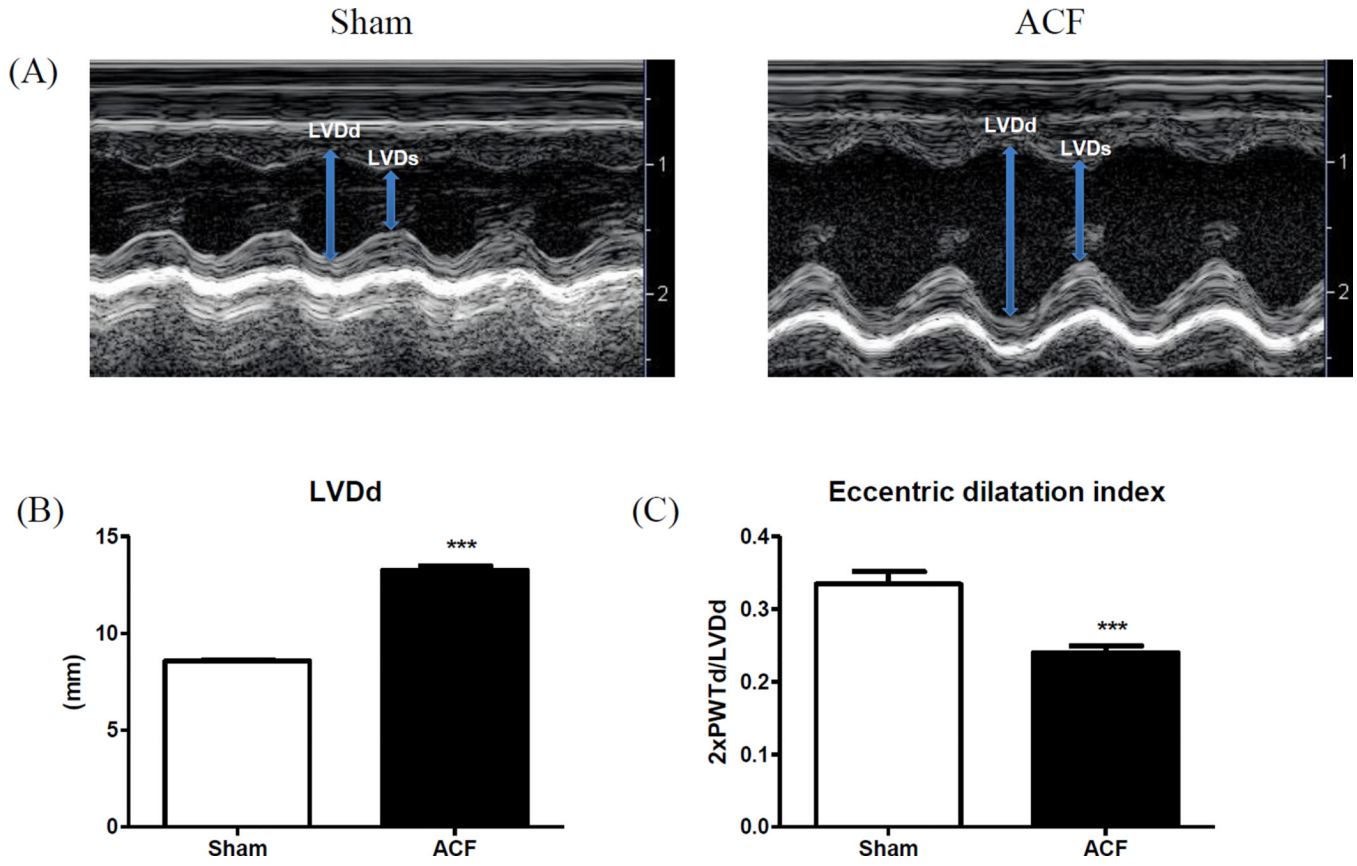

Figure 1.

LV structural remodeling. (A) Representative M-mode images and (B) cumulative data for LV end-systolic and end diastolic diameters (LVDs and LVDd, respectively). (C) Eccentric dilatation index (2xPWTd/LVDd). ***$p<0.001$.

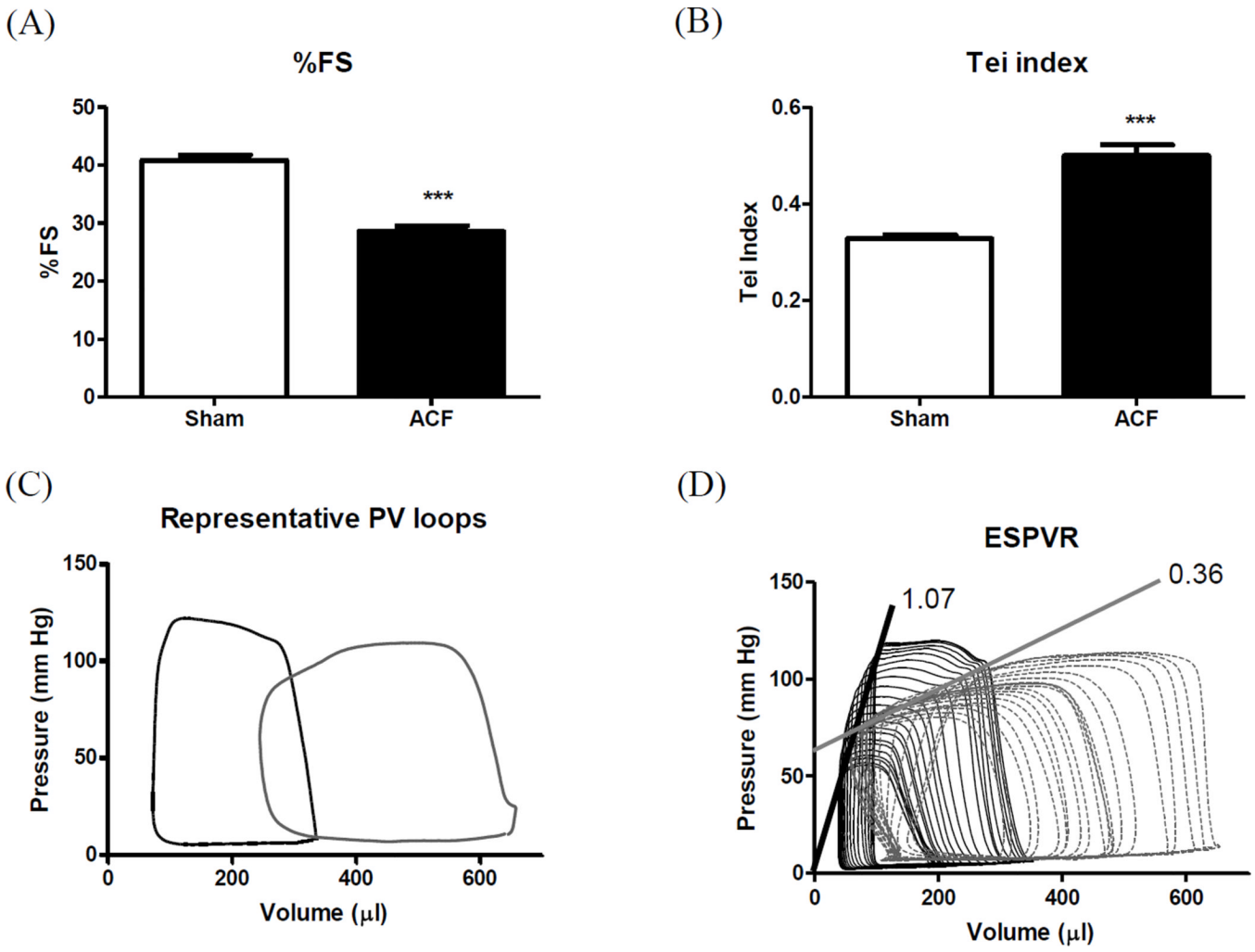

Figure 2.
LV function. (A) %Fractional shortening; (B) Tei index; (C) Representative pressure-volume loops and (D) slope of ESPVR. ***$p<0.001$.

A: Cardiomyocyte function

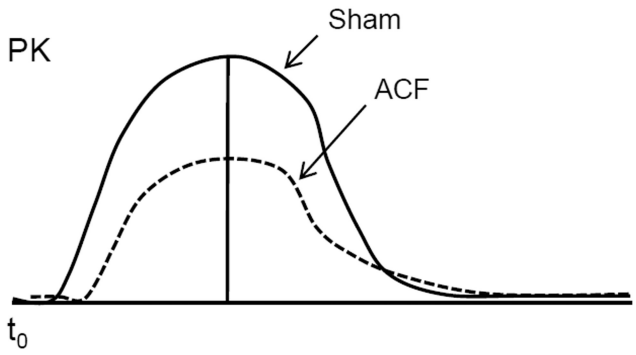

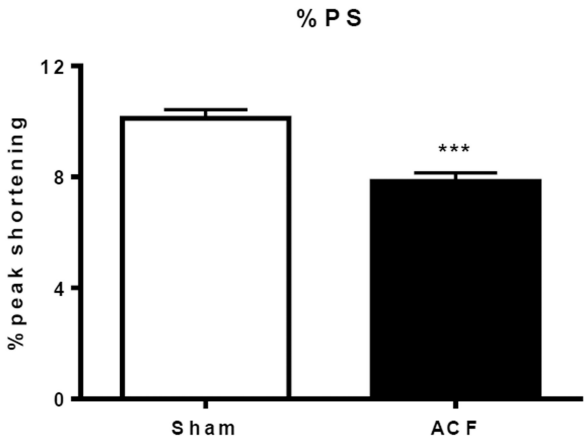

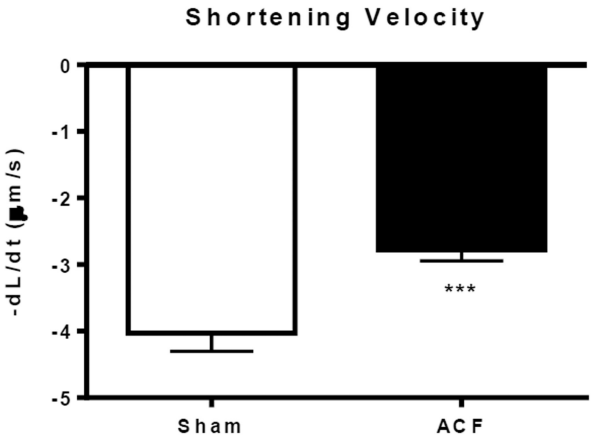

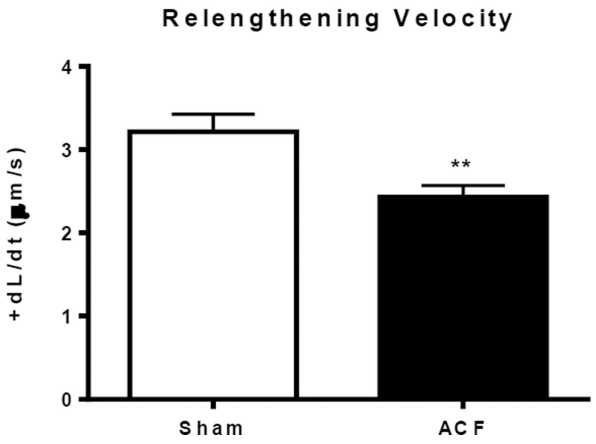

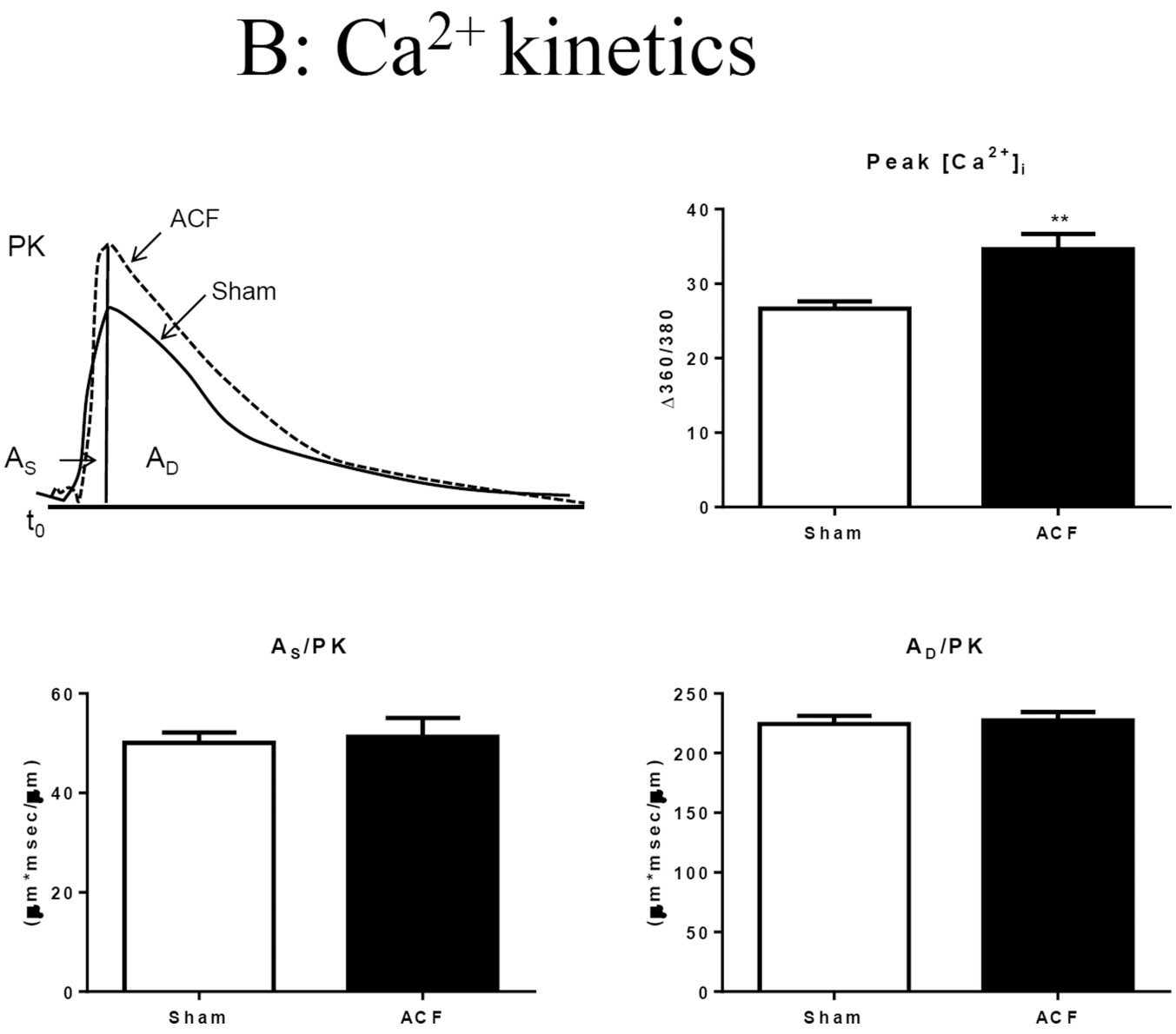

Figure 3.

Single cell shortening and Ca^{2+} transients in 21-wk Sham and ACF myocytes. (A) Top panel: Representative sarcomere shortening in sham and ACF on the left, bar graph to the right. Bottom panel: Velocity of shortening (+dL/dt) and relengthening (-dL/dt). ***p<0.001. (B) Top panel: Representative Ca^{2+} transients from sham and ACF myocytes (left) and intracellular calcium amplitude (peak [Ca_i^{2+}]) in response to electrical stimulation (right). **p<0.01. Bottom panel: Ca^{2+} transient, area under the curver for systolic phase (A_S/PK) and area under the curve for cytosolic Ca^{2+} decay (A_D/PK) normalized to peak. Data represent mean±SEM from 20–30 cells from 4–5 rats/group.

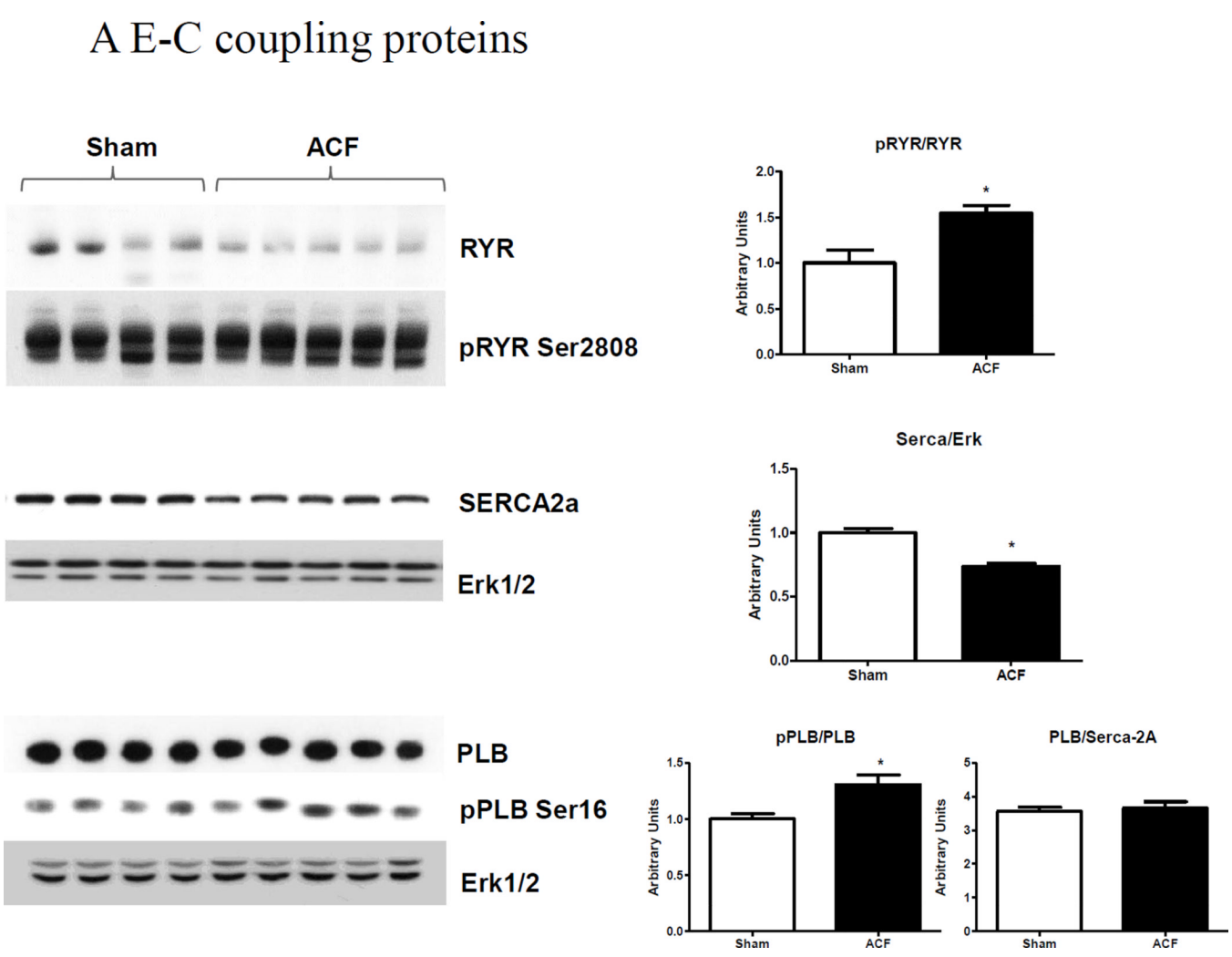

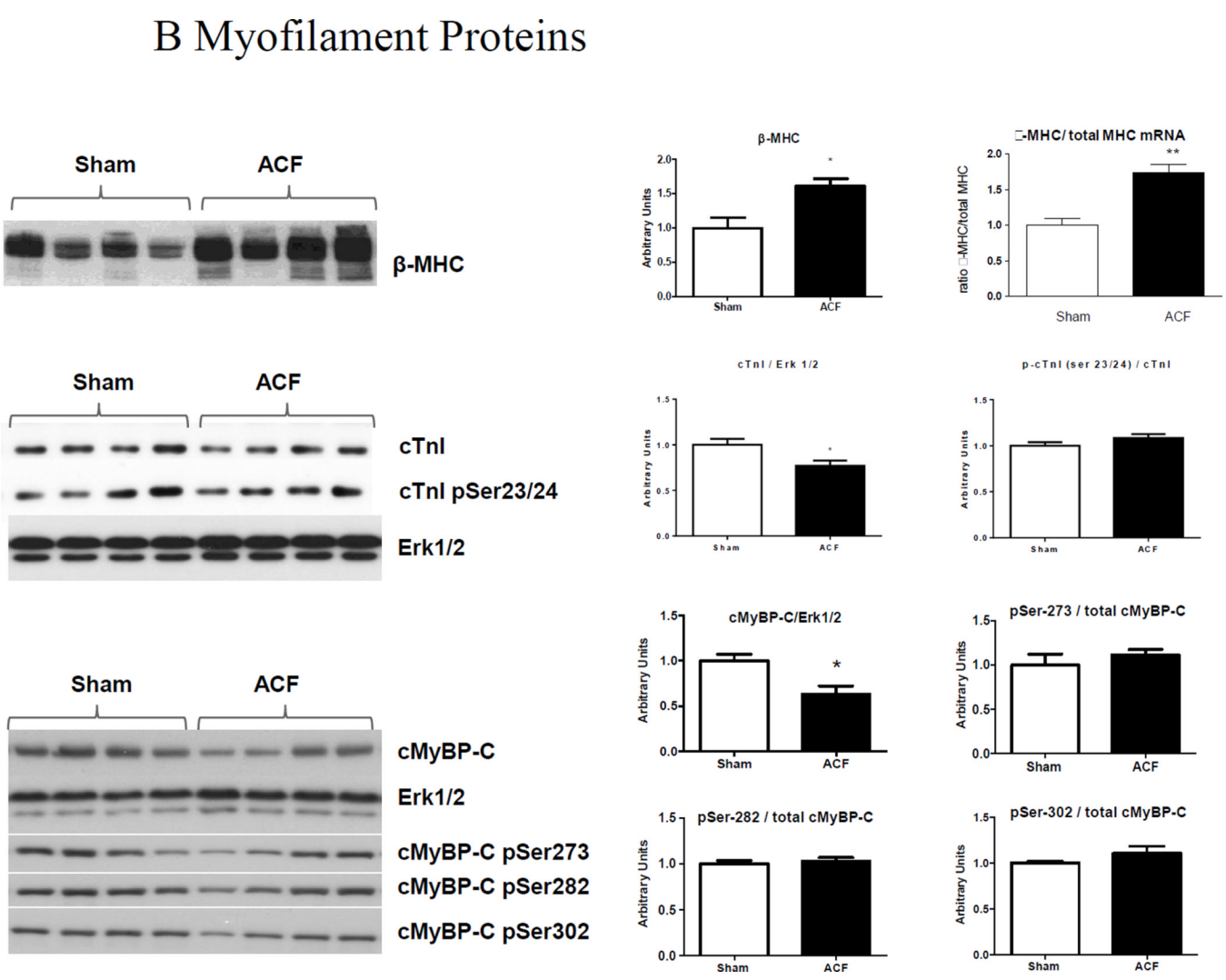

Figure 4.

LV protein analyses. (A) E-C coupling proteins. Representative immunoblots (left) and cumulative data (right) of RyR, phospho-RyR2808, SERCA-2a, PLB and phospho-PLB Ser16 expression. (B) Myofilament proteins. Ratio of β-MHC to total MHC mRNA and representative blots (left) and cumulative data (right) of β-MHC, TnI and phospho-TnI Ser23/24, cMyBP-C, phospho-cMyBP-C (pSer273, p282 and p302) protein expression. ERK1/2 was used as a lane loading control. (n=4–5 rats/group) *p<0.05, **P<0.01.

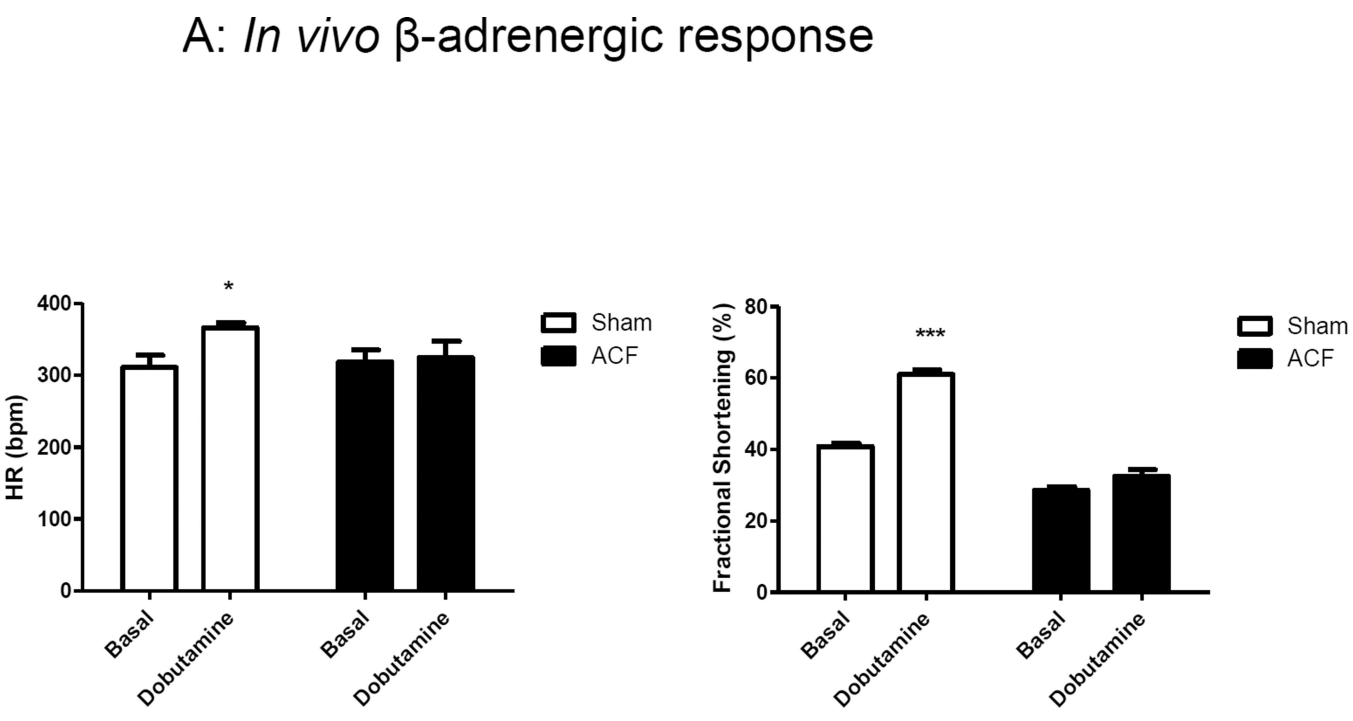

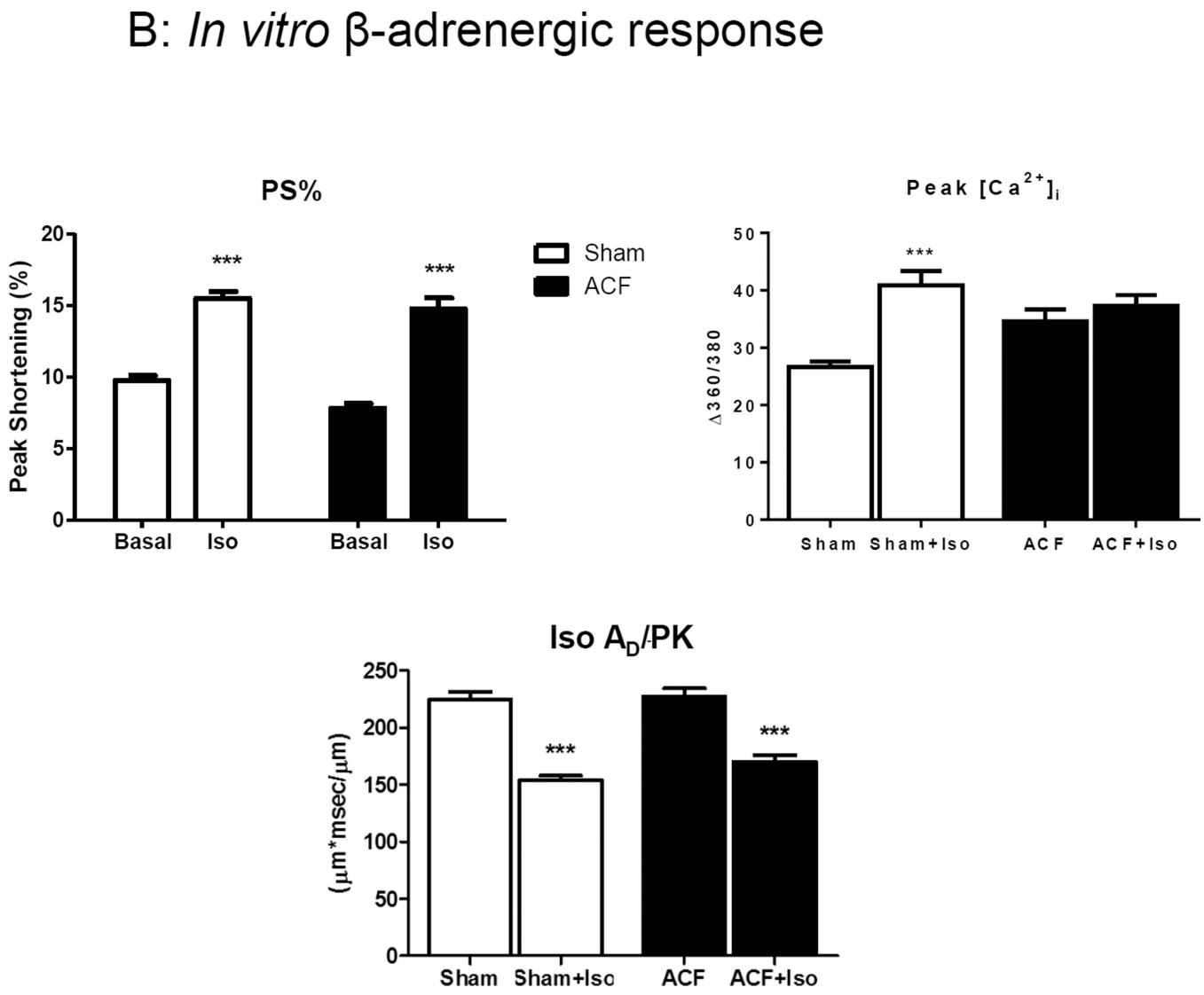

Figure 5.

In vivo and *in vitro* β-adrenergic responsiveness. (A) *In vivo* response to dobutamine in ACF versus sham. (B) *In vitro* responses Iso. Iso had decreased the area under the curve for cytosolic Ca^{2+} decay phase (A_D/PK) in both Sham and ACF groups. ***$p<0.001$.

A- β-AR receptor expression

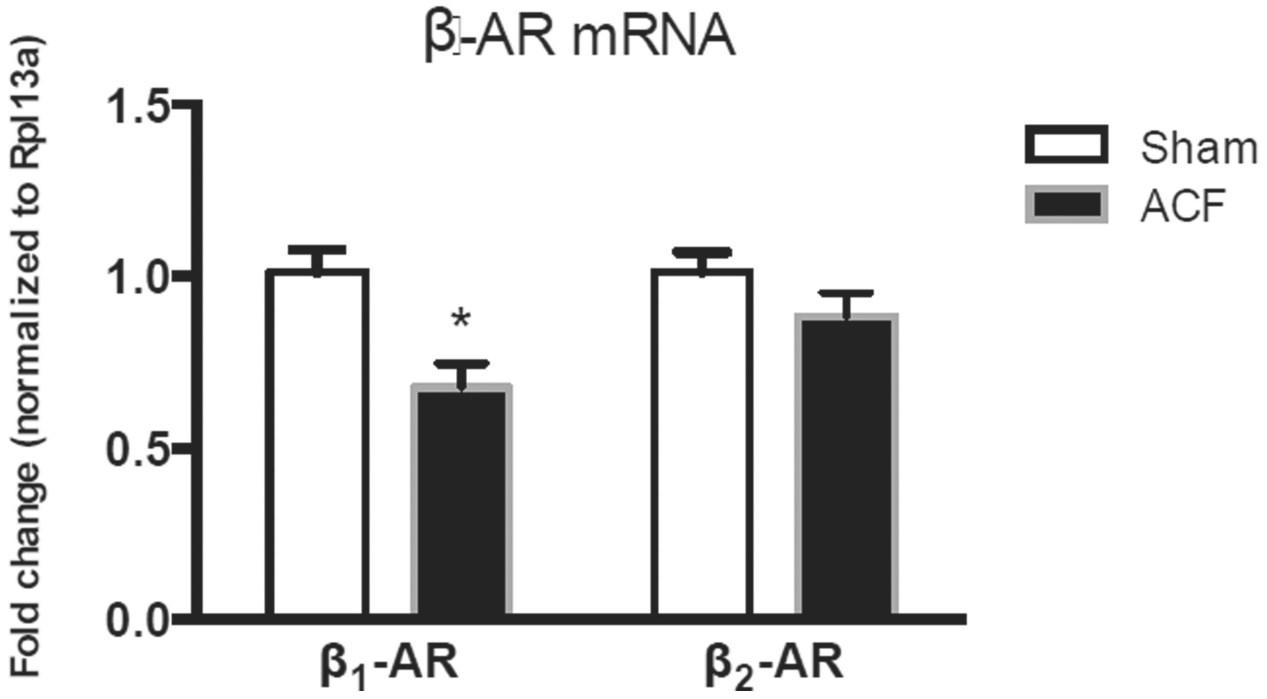

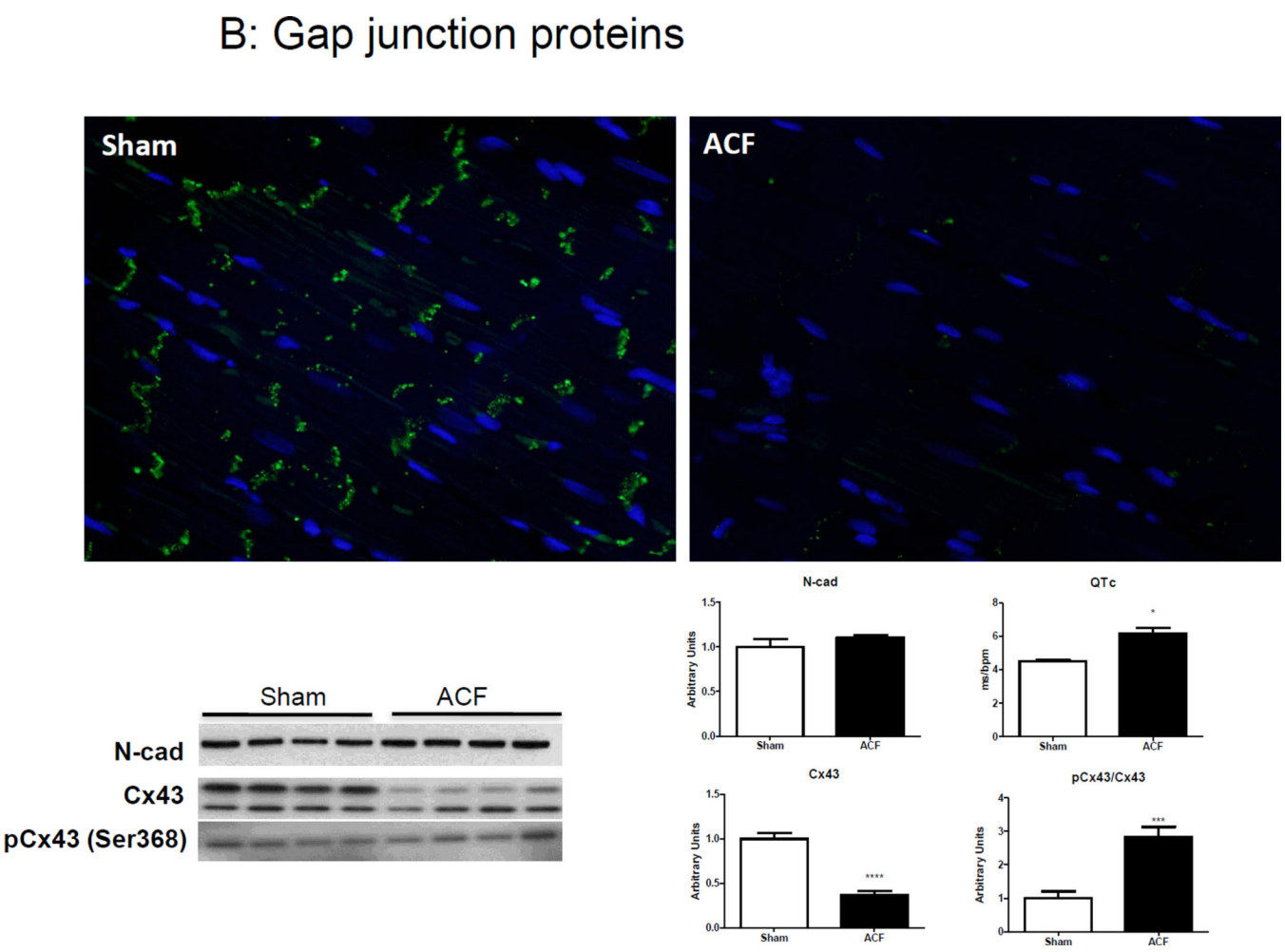

Figure 6.

(A) β_1 and β_2-adrenoceptor mRNA expression. (B) Top Panel: Representative photomicrographs of connexin-43 and N-cadherin staining. Bottom panel: Representative immunoblots (left) and histograms (right) showing quantification of N-cad, Cx-43 and phosphor-Cx43 Ser368. Note elongated QT interval in ACF animals. (B) Representative immunoblots (left) and cumulative data (right) for Src and ZO-1, normalized to ERK1/2 expression. (n=4–5 rats/group) *$p<0.05$.

Table 1

Echocardiographic parameters

	Sham	ACF
N	9	10
LVDd (mm)	8.68±0.14	13.4±0.16***
LVDs (mm)	5.13±0.12	9.42±0.28***
PWTd (mm)	1.54±0.05	1.61±0.05
PWTs (mm)	2.51±0.10	2.35±0.08
FS (%)	41±1	29±1***
Tei Index	0.33±0.01	0.50±0.02***
2xPWTd/LVDd	0.33±0.02	0.24±0.01**
E/A	1.16±0.03	1.23±0.05

LV echocardiography parameters in sham and ACF at 21weeks. LV diameter in diastole and systole (LVDd and LVDs, respectively); Posterior wall thickness in diastole and systole (PWTd and PWTs, respectively); Percent fractional shortening (%FS); Eccentric dilatation index (2xPWTd/LVDd); Mitral E/A ratio. Data are expressed as mean±SEM.

** $p<0.01$,

*** $p<0.001$.

Table 2

Left ventricular morphology and hemodynamic parameters

	Sham	ACF
N	5	5
HW/BW	2.33±0.10	4.57±0.29***
LW/BW	1.73±0.06	3.32±0.25***
HR (bpm)	311±17	319±16
MAP (mmHg)	110±3	101±4
SV (μl)	182.5±8	307±41*
EDV (μl)	299±11	642±55***
ESV (μl)	116±17	335±32***
EF (%)	65±4	47±4*
EDP (mmHg)	8±1	8±1
ESP (mmHg)	117±8	96±8
dP/dt_{max}	6978±828	8106±588
dP/dt_{min}	6858±367	5394±672
Tau (Weiss)	11±0.6	11±1
ESPVR	0.73±0.05	0.32±0.05***
PRSW (mmHg)	93±11	90±11

Left ventricular morphological and hemodynamic parameters. Heart failure indices: Heart weight/body weight (HW/BW) and Lung weight/body weight (LW/BW). Hemodynamic parameters: Heart rate (HR; beats per minute); Mean arterial pressure (MAP); Stroke volume (SV); End diastolic and systolic volumes (EDV and ESV, respectively); Percent ejection fraction (%EF); End diastolic and systolic pressures (EDP and ESP, respectively); change in maximum rate of pressure rise and decline (dP/dt_{max} and dP/dt_{min}, respectively); relaxation constant (tau Weiss); ventricular end systolic elastance (Ees); and Pre-recruitable stroke work (PRSW).

* $p<0.05$,

** $p<0.01$,

*** $p<0.001$.

Table 3

Ca^{2+} kinetics

	Sham	ACF	Sham+Iso	ACF+Iso
+dV/dt	13.80±0.66	20.70±1.63 **	37.32±3.63 ### *(170.43)*	30.63±1.42 ### *(26.61)*
TP 90%	0.04±0.01	0.04±0.002	0.038±0.003 *(6.51)*	0.028±0.001 ## *(−19.06)*
Peak $[Ca^{2+}]_i$	26.7±0.9	34.6±2.1 **	41.3±2.6 *(54.78)*	37.3±1. 9 *(6.52)*
TR 90%	0.50±0.02	0.52±0.02	0.34±0.01 ### *(−31.92)*	0.38±0.01 ### *(−41.22)*
−dV/dt	−1.27±0.09	−1.62±0.11 *	−4.031±0.218 ### *(217.15)*	−2.962±0.137 ### *(33.27)*

Myocyte Ca^{2+} kinetics. Contraction velocity (+dV/dt, speed at which $[Ca^{2+}]_i$ increases); time to peak 90% (TP 90%, time to 90% $[Ca^{2+}]_i$ elevation); peak amplitude (% change in $[Ca^{2+}]_i$ during contraction); time to 90% relengthening (TR 90%, time to remove 90% $[Ca^{2+}]_i$ towards baseline); relaxation velocity (−dV/dt, speed at which $[Ca^{2+}]_i$ declines). Numbers in parentheses indicate %increase in response to Iso.

* $p<0.05$,

** $p<0.01$ versus sham;

\#\# $p<0.01$,

\#\#\# $p<0.001$ vs. respective baseline.